Propofol inhibits inflammatory response by regulating the miR-494/ Nrdp1 pathway in ICH mice model

Hui Shi
neurology
Qijiang Xiong
neurology
Zhongyan Huang
neurology
zhao yang (yangzhao5140@sohu.com)
Neurological Institute https://orcid.org/0000-0002-8398-7159

Research

Keywords: propofol, inflammatory response, miR-494, ICH

Posted Date: February 26th, 2020

DOI: https://doi.org/10.21203/rs.2.24619/v1

Abstract

Background: Propofol is an anesthetic agent with neuro-protective effect in neuronal injury. However, the mechanism of propofol in M1 macrophage polarization following ICH has not been well studied. Ubiquitination mediated M1/M2 macrophage polarization plays important roles in pathogenesis of immune disease. The experiment analyzed anti-inflammatory effects of propofol in macrophages following ICH.

Methods: In the experiment, macrophages were administrated with erythrocyte lysates, and then miR-494, Nrdp1 and M1 related markers were analyzed. In addition, brain inflammatory response, brain edema, and neurological functions of ICH mice were also assessed.

Results: We found that propofol decreased miR-494 levels while increased Nrdp1 levels in macrophages after ICH. We also demonstrated that miR-494 inhibited Nrdp1 expression by directly binding its 3'-untranslated region. MiR-494 attenuated Nrdp1 levels and downstream proinflammatory factors production. Upregulation of Nrdp1 in macrophages significantly decreased M1 macrophage polarization.

Conclusion: Taken together, these results suggest that propofol can attenuate the neuroinflammatory response of macrophages after ICH through regulation of the miR-494/Nrdp1 pathway.

Background

Macrophage mediated inflammatory resnponse plays an important role in hemorrhagic brain damage (1–3). Macrophages are highly plastic cells that can display diverse phenotypes and exert various functions according to specific microenvironmental signals. M1 phenotype macrophage releases proinflammatory mediators and leads to tissue damage. M2 phenotype macrophage generates anti-inflammatory cytokines and contributes to neuroprotective properties (4–6).

Propofol is an intravenous hypnotic agent utilized in anesthesia and intensive care (7). Propofol acts by potentiating the γ-aminobutyric acid type A (GABA-A) receptor-mediated inhibition in the central nervous system (8). In addition, propofol has been identified to play neuroprotective role by anti-inflammatory properties in brain injury (9–11). However, whether propofol contributes to M1/M2 macrophage polarization following ICH and the specific molecular mechanism has not been studied.

miRNAs are small noncoding (NC) RNA molecules (~ 20–22 nucleotides) and contribute to mRNA post-transcriptional regulation(12–14). In recent years, miRNAs have acted as potential biomarkers in inflammatory diseases (15). In addition, miRNAs are involved in the development and regulation of both innate and adaptive immunity and contribute to regulate M1/M2 macrophage polarization (16–18). Recent studies have suggested that altered expression of miR-494 contributed to several inflammation-mediated diseases (19). Notably, targeting miR-494 has been found to be potential biomarker and therapeutic target to the inflammatory response.

Ubiquitination is a common post-translational modification of protein and regulates many cell processes, such as growth, cycle, and apoptosis (20). Ubiquitination has also been identified in many aspects of immune responses (21). Nrdp1, an E3 ubiquitin ligase, has previously been demonstrated to inhibit M1 activation of macrophages (22).

In this experiment, we made a hypothesis that the miR-494 signaling pathway contributes to the protective roles of propofol in ICH-induced neuroinflammation. Erythrocyte lysates-treated macrophages and ICH mice have been used as an in vitro and in vivo model to study the mechanisms underlying neuronal injury. The results demonstrated that propofol could attenuate pro-inflammatory mediator production by downregulating miR-494 levels, which targeted Nrdp1 signaling pathways.

Methods

Animals

8 week-old male specific pathogen-free (SPF) C57BL/6 mice were purchased from Chongqing Medical University and were housed in standard polypropylene cages at the animal facility until the day of the experiment. All procedures were performed in accordance with guidelines established by the Animal Care and Use Committee of Chongqing Medical University.

Macrophage culture

BMDMs (bone marrow derived macrophages) were isolated from the marrow of the femurs and tibias of C57BL/6 mice. The legs of the animals were sprayed with 70% EtOH, and the skin and muscle tissue were removed from the bones. The bones were sprayed with 70% EtOH, transferred to a sterile-flow hood and cut at both ends. The marrow was flushed out into a sterile falcon tube in Dulbecco's modified Eagle's medium supplemented with heat-inactivated fetal bovine serum (FBS; 50 ml; 10%) and penicillin-streptomycin (5 ml; 1%; Gibco). The cell suspension was triturated using a sterile Pasteur pipette, filtered through a nylon mesh filter into a sterile tube and centrifuged (400 × g, 5 min). The supernatant was removed, and the pellet was resuspended in red blood cell lysis buffer (Sigma-Aldrich, Gillingham). The suspension was centrifuged (400 × g, 5 min), the supernatant was discarded and the cells were washed using DMEM and centrifuged once more (400 × g, 5 min). The pellet was resuspended in 20 ml of DMEM supplemented with L929-conditioned media (20%). Cells were seeded in sterile cell culture flasks (T175 cm^2 flasks). On day 2, non-adherent cells were removed from the flask, the media was replaced and the remaining adherent cells were maintained in culture for a further 6 days.

Neuronal cultures

Cortical neuronal were prepared from embryonic day 16–18 C57BL/6 mice. Briefly, the cerebral cortices and hippocampus of fetus mice were dissected out and the meninges were carefully removed. Cells (1×10^6 cells/mL) were maintained in poly-d-lysine (Sigma, St. Louis, MO) coated plates in Dulbecco's modified eagle medium (DMEM) medium (Life Technologies) with 10% fetal bovine serum (FBS) (Life

Technologies). After 4–6 h of culture, the cultures were replenished with Neurobasal medium (Life Technologies) containing 100 U/mL penicillin, 100 µg/mL streptomycin, 2% B27, and 0.5 mM glutamine (Life Technologies) at 37 °C with 5% CO_2. The medium was changed every three days.

Preparation of erythrocyte lysates

Whole blood collected from 30 to 50 mice was pooled and leuko reduced using a Neonatal High-Efficiency Leukocyte Reduction Filter (Purecell Neo; Pall Corporation). Blood was centrifuged at 400 × g for 15 minutes, and the volume reduced to a final hemoglobin level ranging from 17.0 to 17.5 g/dL, as determined by a modified Drabkin hemoglobin assay at a 1:251 dilution of stored RBCs to Drabkin reagent (Ricca Chemical Company). Washed stored RBCs were prepared with 3 washes using 10 volumes of phosphate-buffered saline (PBS) and centrifugation at 400 g. After the final wash, the washed stored RBCs were resuspended in PBS to a final hemoglobin concentration of 17.0 to 17.5 g/dL for transfusion. Supernatant was obtained using a 400gspin of stored RBCs and 400 µL of this solution were transfused undiluted. RBC ghosts were obtained by hypotonic lysis of twice the volume of stored RBCs (ie, for 400 µL of ghosts, 800 µL of stored RBCs were hemolyzed) with PBS to distilled water (1:15), followed by multiple washes with the same buffer and centrifugation at 30 000 g until a white pellet was obtained. The white pellet of RBC ghosts was resuspended in PBS. Stroma-free RBC lysate was prepared by freeze-thaw of washed stored RBCs followed by centrifugation at 16 000 × g to pellet and remove the stroma.

Cell treatment

Macrophages (1×10^5) were stimulated with propofol (0 ~ 100 µM) plus 10 µl PBS or erythrocyte lysates for 24 hs. After then, the supernatants were removed and further analyzed for cytokine production with ELISA.

Real-time PCR

The ipsilateral hemisphere was homogenized using RNAiso Plus (Takara) and ceramic beads for 1 min in a speedmill plus according to the instructions of the manufacturer (Alytik Jena). RNA was isolated according to the instructions of the manufacturer and reverse transcripted to obtain cDNA using a PrimeScript™ RT Reagent Kit with gDNA Eraser (Takara). Real-time PCR was performed using cDNA samples with SYBR@Premix ExTaq™II (Takara, Tli RNaseH Plus) by the One-step Plus analyzer (ABI). We normalized the results for each individual gene using the housekeeping gene beta-actin. The $2^{-\Delta\Delta CT}$ method was used to calculate relative gene expression levels.

Western blotting analysis

Proteins from cultured macrophages were resolved using SDS-PAGE and transferred onto polyvinylidene fluoride membranes using electroblotting. The membranes were incubated with primary antibodies, all diluted to 1:1000 (Cell Signaling Technology), at 4˚C overnight. GAPDH (1:200; Santa Cruz Biotechnology, Dallas, TX) was used as the loading control. The membranes were incubated with HRP-conjugated goat

anti-rabbit secondary Abs (1:2500; Sigma-Aldrich, St. Louis, MO) at 25˚C for 1 h. Bound Abs were visualized using a chemiluminescence detection system. Protein levels were calculated as the ratio of the target protein value to the GAPDH value.

Enzyme-linked immunosorbent assay

The supernatants or brain tissue extracts were harvested, and TNF-α, IL-1β and IL-6 productions were determined by ELISA. The specimens were assayed using respective Enzyme Linked Immunosorbent Assay (ELISA) kits (Minneapolis, MN, USA) according to the instruction manuals.

Cytotoxicity assay

The cytotoxic activity of macrophages was measured by a 6 h lactate dehydrogenase release assay using CytoTox96 Non-radioactive Cytotoxicity Assay kit (Promega, Charbonnie'res-les-Bains, France) on 5×10^3 neuron/well. Neuron was then added to the wells with 2×10^3 macrophage. Experiments were performed in quadruplet and the percentage of lysis was determined by OD490 measurement as described in the manufacturer's instructions. The percentage of cell mediated cytotoxicity was calculated according to the equation: % Specific Lysis = (effector/target cell mix LDH release-spontaneous effector LDH release)/(maximum target LDH release - spontaneous target LDH release) × 100%:

Oligonucleotide transfection

All of the transient transfections were performed with Lipofectamine 2000 Reagent (Invitrogen). MiRNA oligonucleotide transfections were performed according to an established protocol. Briefly, macrophages were seeded in 6-well plates at a density of 2×10^5 cells per well and were grown overnight to 60%-80% confluency. Next, miRNA mimic (Pre-miR ™ miRNA precursor) or miRNA inhibitor (Anti-miR ™ miRNA inhibitor) (Ambion) was added to the culture media at a final concentration of 100 nM according to the manufacturer's recommendations. The sequences of miR-494 used were shown as following: miR-494 mimic, 5'-UGAAACAUACACGGGAAACCUC-3', miR-494 inhibitor, 5'-UUCUCCGAACGUGUCACGUUU-3'. Transfection efficiency (> 90%) was measured by qRT-PCR. For small interfering RNA (siRNA) inhibition were purchased from Santa Cruz Biotechnology (Santa Cruz, CA) and were introduced into the macrophage at final concentrations of 100 nM according to the siRNA transfection protocol. Control siRNA-transfected macrophages were used as the negative control. Transfection efficiency (> 80%) was measured by qRT-PCR. After 6 h of transfection, the medium was replaced with normal glucose or low-serum (2% FBS) medium and cells were incubated for 48hs.

Vector construction and luciferase reporter assays

Luciferase reporter constructs were used, and luciferase assays were performed as described previously. Briefly, the mouse Nrdp1 3'-UTR sequence was amplified by PCR from mouse genomic DNA, and ligated into the pMIR-REPORT luciferase vector multiple cloning site (Ambion, Austin, TX) to yield pMIR- Nrdp1 3'-UTR (NRDP1 3'-UTR). Another pMIR-REPORT luciferase construct containing the Nrdp1 mRNA 3'-UTR with

a mutation by site-directed mutagenesis was generated as a negative control and named Mut- Nrdp1 3'-UTR. Macrophage were plated in 6-well plates and allowed to reach 60%-80% confluence overnight. Cells were then co-transfected with a reporter construct (pMIR-null REPORT plasmid, pMIR- Nrdp1 3'-UTR, pMIR-Nrdp1 3'-UTR-Mut). After 24 h, cells were harvested, and luciferase activity was measured using the Dual-Luciferase Reporter Assay System (Promega) according to the manufacturer's recommendations. Luciferase activity was normalized to control TK Renilla construct expression (pRL-TK, Promega).

ICH model

After anesthetizing mice with 1–3% isoflurane inhalation and ventilating them with oxygenenriched air (20%:80%), we injected a total of 0.5 μL containing 0.075 units of collagenase VII-S (No. C9572, Sigma, St. Louis, MO) at 0.1 μL/min into the left basal ganglion at the following coordinates relative to bregma: 0.8 mm anterior, 2 mm lateral, and 2.8 mm deep. The craniotomy was sealed with bone wax, and the scalp was closed with 4 − 0 silk sutures. Rectal temperature was maintained at 37.0 ± 0.5 °C throughout the experimental and recovery periods (DC Temperature Controller 40-90-8D; FHC Inc., ME). Sham-operated mice received the same treatment, including needle insertion, but collagenase was not injected. The mortality rate in untreated animals is 4.6%.

Intracerebroventricular injection

To investigate the anti-inflammatory effects of propofol, propofol (2 μg/2 μl) or PBS (2 μl) was pretreated with a single intracerebroventricular (i.c.v.) injection in the ipsilateral ventricle 15 min before ICH. For the injection into the ipsilateral ventricle, a small burr hole was made in the parietal region (1.0 mm posterior and 1.0 mm lateral to the bregma) under the guidance of the stereotaxic instrument (RWD Life Science).

Histochemical evaluation of microphage activation

3 days after ICH, the animals were deeply anaesthetized with pentobarbital and transcardially perfused with 0.9% saline followed by 4% paraformaldehyde in 0.1 M phosphate buffer (PB,pH7.4). After the mice were perfused and fixed, the perihaematomal region of cerebral tissues were collected, fixed in 4% paraformaldehyde for 24 h, dehydrated in 30% sucrose solution for 48 h, embedded, frozen, and cut into 25-μm sections using a Leica CM1900 cryostat. The perihaematomal region was treated with 3% H_2O_2 in 0.01 M phosphate-buffered saline (PBS) and preincubated in 5% normal goat serum. The samples were then incubated in a primary antibody solution containing rat anti- Iba antibody (Serotec, Fullerton, CA, USA, 1:200) overnight at 4 ◦ C. After washing, the samples were incubated in a secondary IgG antibody (1:200) for 1 h at room temperature (RT). Finally, the sections were incubated in horseradish peroxidase (HRP)-Streptavidin (1:200) for 1 h at RT, and the colour reaction was conventionally developed with diaminobenzidine (DAB) and H_2O_2. For each animal, six representative sections of each brain were selected. IPP6.0 image processing software (Media Cybernetics, MD, USA) was utilized to count the number of positive cells.

Evans Blue Extravasation

Briefly, the Evans blue dye (2%, 5 mL/kg; Aladdin, Shanghai, China) was injected and administered > 2 minutes into the left femoral vein under anesthesia, where it was allowed to circulate for 60 minutes. Then mice were euthanized by an intracardial perfusion with sterile saline. Then brain samples were weighed, homogenized in sterile saline, and centrifuged at 15000 g for 30 minutes. After that, equal volume of trichloroaceticacid was added to the resultant supernatant. Those samples were then incubated overnight at 4 °C and centrifuged again at 15000 g for 30 minutes. The resultant supernatant was spectrophotometrically quantified for the extravasated Evans blue dye at 620 nm.

Evaluation of neurological scores

A standardized battery of behavioral tests was used to quantify neurological function at 3ds post-ICH. The neurological scores were determined by Neurological Severity Scores, a composite of motor, sensory, reflex, and balance tests. Neurological function was graded on a scale of 1–18; a score of 1 point is awarded for the inability to perform the test or for the lack of a tested reflex. The higher the score, the more severe the injury (normal score 2–3; maximal deficit score 18). Tests were conducted by an observer blinded to the treatment group.

Brain water content measurement

Brain water content was measured in mouse cerebral tissues after ICH. Briefly, mice were randomly sampled from each group and anesthetized by intraperitoneal injection with chloral hydrate (n = 5). Next, the cerebral tissues were removed, and the surface water on the cerebral tissues was blotted with filter paper. Brain samples were immediately weighed on an electric analytic balance to obtain the wet weight and then dried at 100 °C for 24 h to obtain the dry weight. Brain water content was calculated using the following formula: brain water content (%) =(wet weight - dry weight) / wet weight × 100%.

Statistical Analysis

All experiments were independently performed three times. The differences between groups were determined with the one-way analysis of variance (ANOVA) using SPSS 13.0 software. P values of less than 0.05 were considered to be statistically significant.

Results

Propofol attenuates erythrocyte lysates-induced M1 polarization

To explore the effects of propofol on erythrocyte lysates-induced macrophage polarization, macrophages were pretreated with various concentrations of propofol and stimulated with erythrocyte lysates for 24 hs. The results showed that stimulation of erythrocyte lysates increased the production of TNF-α and IL-1β respectively. However, these pro-inflammatory factors were significantly inhibited by propofol in a concentration-dependent manner (Fig. 1). The data demonstrated that propofol attenuated erythrocyte lysates-induced M1 polarization.

Propofol suppresses erythrocyte lysates-induced miR-494 levels

Recent studies indicated that miR-494 contributes to the regulation of inflammation and innate immune responses. Thus, we investigated miR-494 levels on erythrocyte lysates stimulation by using a real-time PCR assay. The treatment of macrophages with erythrocyte lysates showed increased miR-494 levels. To test the hypothesis that propofol downregulates inflammation by targeting miR-494, macrophages were pretreated with various concentrations of propofol and stimulated with erythrocyte lysates. The results demonstrated that miR-494 levels decreased after erythrocyte lysates treatment compared with control groups (Fig. 2). The data suggests that propofol suppresses erythrocyte lysates-induced miR-494 levels.

MiR-494 is required for propofol inhibition of inflammation

To further assess the role of miR-494 in the anti-inflammation of propofol, miR-494 inhibitor was used to inhibit miR-494 levels in macrophages. Macrophages were transduced with miR-494 inhibitor or controls, and the inhibition was assessed by real-time PCR. The miR-494 levels were significantly decreased in the cells treated with the miR-494 inhibitor compared with controls (Fig. 3A). Next, we detected the pro-inflammatory factors levels of macrophages after propofol treatment, and found that these cytokines decreased in miR-494 knockdown group compared with controls (Fig. 3B). The data indicate that miR-494 is critical to the anti-inflammation of propofol.

Nrdp1 was a direct target of miR-494 in macrophage The target prediction program TargetScan (www.targetscan.org) suggests 3'-UTR of Nrdp1 mRNA includes a putative miR-494 target sequence (Fig. 4A). To identify Nrdp1 was a direct target of miR-494 in macrophages, we analyzed this relationship by a Dual-Luciferase reporter system. Our data found that co-expression with miR-494 mimics significantly attenuated the activity of a firefly luciferase reporter containing wild-type Nrdp1 3' -UTR, while miR-494 mimics could not attenuate the activity of a firefly luciferase reporter containing a mutated Nrdp1 3 '-UTR (Fig. 4B). The phenomenon suggested that miR-494 likely attenuated Nrdp1 expression by directly binding target sites in the Nrdp1 3'-UTR.

Propofol upregulates Nrdp1 by suppressing miR-494

In addition, we investigated whether propofol inhibition of miR-494 would increase Nrdp1 levels. The Nrdp1 levels of macrophage were evaluated after different treatments. We detected Nrdp1 levels of macrophages after propofol treatment, and found that Nrdp1 levels increased compared with controls (Fig. 5A). In addition, macrophages were transduced with miR-494 or controls, and further treated by propofol. The results demonstrated that the increased levels of Nrdp1 were not significant after miR-494 transduction. However, levels of Nrdp1 were much more robust after miR-494 inhibitors transduction (Fig. 5B). The results suggest that propofol upregulates Nrdp1 by suppressing miR-494.

Downregulation of Nrdp1 attenuates the anti-inflammatory effects of propofol

To explore the role of Nrdp1 in propofol mediated anti-inflammatory effect, we detected cytokine levels in macrophage in which Nrdp1 was downregulated. Macrophages were transduced with Nrdp1 siRNA or

control siRNA, and the inhibition efficiency was assessed by Western blot. Nrdp1 levels were significantly decreased in Nrdp1 siRNA group compared with control group (Fig. 6A). TNF-α and IL-6 production of macrophages transduced with Nrdp1 siRNA after erythrocyte lysates treatment was significantly increased compared with macrophages transduced with control siRNA (Fig. 6B). Therefore, Nrdp1 plays an important role in the anti-inflammatory activity of propofol.

Propofol attenuated macrophage accumulation of the perihematomal region

Macrophage accumulation was involved in the brain inflammatory damage. To detect the effect of propofol in macrophage accumulation, we detected the Iba-1-positive macrophages in the perihematomal brain tissue at 3 days after ICH. Our data indicated that the number of macrophage in the perihematomal brain tissues increased at 3 days in ICH mice compared with sham controls. However, the number of macrophage in ICH mice after propofol treatment decreased compared with that in control ICH mice (Fig. 7A). These results suggested that propofol attenuated macrophage accumulation of the perihematomal region in ICH mice.

Propofol inhibits inflammatory injury in vivo. To explore the role of propofol to neurological function, i.c.v. adminstration of propofol or PBS were administered 10 min after ICH. BBB integrity, Brain water content and neurological injury of mice were observed 3 days after ICH. We found that propofol significantly inhibited BBB injury, water content and neurological damage (Fig. 7B-D). These data suggested that propofol could inhibit inflammatory injury in vivo.

Discussion

Spontaneous intracerebral hemorrhage (ICH) is a subtype of stroke, accounting for 15 to 20% of all stroke types. While the high mortality and morbidity makes ICH a challenging problem, there are no effective therapies for ICH patients (23–25). Much study demonstrates that inflammatory responses are involved in the progress and progression of brain injury following ICH, including macrophage activation and neutrophil infiltration (26–28). Various factors, such as thrombin and glutamate, could activate macrophages and elicit inflammatory response, and subsequently generate neuroinflammation following ICH (29–31). Therefore, the strategies based on inhibition of macrophage activation might represent promising way for ICH.

Macrophage produces nutrition factors and nerve toxicity factors, and shows the dual role of proinflammatory and anti-inflammatory, characterized by M1 and M2 polarization (32–34). M1 macrophage secretes high levels of oxide metabolites and proinflammatory factor, such as IL-6 and TNF-α. Its role is to eliminate pathogenic microorganisms and cancer cells, but also lead to the normal cell and tissue injury (35). M2 macrophage secretes high level of IL-10 and TGF-β. Its role is immune suppression, tissue repair and functional remodeling (36).

Much evidence demonstrated that miRNA level varied in different macrophage polarization. It was also identified that miRNAs contributed to macrophage polarization (37). For example, miR-155 and miR-146a

contribute to M1 polarization and their expressions are promoted by IFN-γ or LPS stimulation (38–39). Recent research demonstrated that miR-21 modulates the polarization of macrophages and increases the effects of M2 macrophages on promoting the chemoresistance of ovarian cancer (40). Propofol is a widely used intravenous anesthetic agent with potential neuroprotective effect in neuronal damage, including ischemic stroke and traumatic brain injury (41–42). However, the effects and molecular mechanisms of propofol in M1 macrophage polarization after ICH have not been identified.

Firstly, we utilized erythrocyte lysates-treated macrophage model to explore the effects of propofol on erythrocyte lysates-induced macrophage polarization. We found that that propofol attenuated erythrocyte lysates-induced M1 polarization. Secondly, we investigated miR-494 levels on erythrocyte lysates stimulation by using a real-time PCR assay. The data suggested that propofol suppressed erythrocyte lysates-induced miR-494 levels and miR-494 is critical to the anti-inflammation of propofol. Thirdly, we identified that Nrdp1 was a direct target of miR-494 in macrophage and propofol upregulated Nrdp1 by suppressing miR-494. Downregulation of Nrdp1 attenuated the anti-inflammatory effects of propofol. Lastly, we proved that propofol attenuated macrophage accumulation of the perihematomal region and significantly inhibited BBB injury, water content and neurological damage following ICH in vivo.

Conclusion:

Our data suggests that propofol can attenuate the neuroinflammatory response of macrophages after ICH through the regulation of the miR-494/Nrdp1 pathway. In addition, propofol also represent anti-inflammatory therapy strategy in ICH.

Declarations

Acknowledgements

None.

Authors’ contributions

Conceptualization: CLZ; Methodology: HS; Manuscript Preparation: ZY. All authors read and approved the final manuscript.

Funding

The study was supported by National Natural Science Foundation of

China (NSFC No. 81870962).

Ethics approval and consent to participate

All animals received care in compliance with the Principles of Laboratory Animal Care and National standards.

Availability of data and materials

Please contact author for data requests.

Consent for publication

Not applicable.

Competing interests

The authors declare that they have no competing interests.

References

1. Peng Yang, Anatol Manaenko, Feng Xu, et al. Role of PDGF-D and PDGFR-β in neuroinflammation in experimental ICH mice model. Experimental Neurology. 2016(283): 157-164.
2. Qun Lin, Jian-Yong Cai, Chuan Lu, et al. Macrophage migration inhibitory factor levels in serum from patients with acute intracerebral hemorrhage: Potential contribution to prognosis. Clinica Chimica Acta. 2017(472): 58-63
3. Qinghua Luo, Dongling Li, Bing Bao, et al. NEMO-binding domain peptides alleviate perihematomal inflammation injury after experimental intracerebral hemorrhage. Neuroscience. 2019(409): 43-57
4. Yin Gao, Peng Fang, Wen-Jin Li, et al LncRNA NEAT1 sponges miR-214 to regulate M2 macrophage polarization by regulation of B7-H3 in multiple myeloma. Molecular Immunology: 2020(117): 20-28
5. Trung H. M. Pham, Susan M. Brewer, Teresa Thurston, et al. Salmonella-Driven Polarization of Granuloma Macrophages Antagonizes TNF-Mediated Pathogen Restriction during Persistent Infection Cell Host & Microbe. 2020.27(18): 54-67.
6. Kamiya Mehla, Pankaj K. Singh. Metabolic Regulation of Macrophage Polarization in Cancer. Trends in Cancer. 2019,5(12): 822-834.
7. Tomohiro Shintaku, Takayoshi Ohba, Hidetoshi Niwa, et al. Effects of Propofol on Electrocardiogram Measures in Mice. Journal of Pharmacological Sciences. 2014. 126, (4):351-358.

8. Chien-Liang Chen, Yea-Ru Yang, Tsai-Hsien Chiu. Activation of rat locus coeruleus neuron GABAA receptors by propofol and its potentiation by pentobarbital or alphaxalone. European Journal of Pharmacology. 1999. 2(315): 201-210.9
9. Hua-bin Zhang, Xian-kun Tu, Quan Chen, et al. Propofol Reduces Inflammatory Brain Injury after Subarachnoid Hemorrhage: Involvement of PI3K/Akt Pathway. Journal of Stroke and Cerebrovascular Diseases. 2019. 28(12) 104375
10. Melissa A. Hausburg, Kaysie L. Banton, Phillip E. Roman, et al. Effects of propofol on ischemia-reperfusion and traumatic brain injury. Journal of Critical Care. 2020(56)281-287.
11. Chunyan Zhang, Yuxia Wang, Jin Jin, et al. Erythropoietin protects propofol induced neuronal injury in developing rats by regulating TLR4/NF-κB signaling pathway abstract. Neuroscience Letters. 2019. 712: 134517.
12. Yi Cao, Jian-Bo Xiong, Guo-Yang Zhang, et al. Long Noncoding RNA UCA1 Regulates PRL-3 Expression by Sponging MicroRNA-495 to Promote the Progression of Gastric Cancer. Molecular Therapy - Nucleic Acids. 2020(196): 853-864
13. Min Liu, Cuiping Shen, Changxiu Wang, et al. Long Noncoding RNA LINC01133 Confers Tumor-Suppressive Functions in Ovarian Cancer by Regulating Leucine-Rich Repeat Kinase 2 as an miR-205 Sponge. The American Journal of Pathology. 2019,189(11): 2323-2339
14. Satya K. Kota, Savithri B. Kota. Noncoding RNA and epigenetic gene regulation in renal diseases. Drug Discovery Today. 2017.22(7): 1112-1122
15. Qianjin Lu, Ruifang Wu, Ruifang Wu, et al. miRNAs as Therapeutic Targets in Inflammatory Disease. Trends in Pharmacological Sciences. 2019,40(11): 853-865.
16. SamueleTardito, GiuliaMartinelli, StefanoSoldano. Macrophage M1/M2 polarization and rheumatoid arthritis: A systematic review. Autoimmunity Reviews. 2019,18(11). 102397.
17. Dong Wang, Xiaohui Wang, Mahan Si, et al. Exosome encapsulated miRNAs contribute to CXCL12/CXCR4-induced liver metastasis of colorectal cancer by enhancing M2polarization of macrophages. Cancer Letters. 2020. 474(1):36-52.
18. A. Kim, P. Saikia, M. Mcmullen, et al. SAT-459: miRNA regulation of macrophage M1/M2 polarization of Kupffer cells and PBMCs in alcoholic liver disease. Journal of Hepatology. 2018.68(1): s813.
19. Yun Ling, Zheng-Zhao Li, Jian-Feng Zhang, et al. MicroRNA-494 inhibition alleviates acute lung injury through Nrf2 signaling pathway via NQO1 in sepsis-associated acute respiratory distress syndrome. Life Sciences. 2018,210(1): 1-8.
20. Jiuhe Zhu, Nien-Pei Tsai.Ubiquitination and E3 Ubiquitin Ligases in Rare Neurological Diseases with Comorbid Epilepsy. Neuroscience. 2020.428(21) 90-99.
21. Diana Gómez-Martín, Mariana Díaz-Zamudio, Jorge Alcocer-Varela.Ubiquitination system and autoimmunity: The bridge towards the modulation of the immune response. Autoimmunity Reviews. 2008, 7(4): 284-290.

22. Shan-shan Liu, Xiao-xi Lv, Chang Liu. Targeting Degradation of the Transcription Factor C/EBPβ Reduces Lung Fibrosis by Restoring Activity of the Ubiquitin-Editing Enzyme A20 in Macrophages. Immunity. 2019, 51(317): 522-534
23. Guoqing Wang, Zhihua Li, Shujian Li, et al. Minocycline Preserves the Integrity and Permeability of BBB by Altering the Activity of DKK1–Wnt Signaling in ICH Model. Neuroscience. 2019 415(1) 135-146.
24. Gurmeen Kaur, Laura K. Stein, Amelia Boehme, et al. Risk of readmission for infection after surgical intervention for intracerebral hemorrhage. Journal of the Neurological Sciences. 2019, 399(15): 161-166.
25. Stefano Forlivesi, Gianni Turcato, Cecilia Zivelonghi, et al. Association of Short- and Medium-Term Particulate Matter Exposure with Risk of Mortality after Spontaneous Intracerebral Hemorrhage. Journal of Stroke and Cerebrovascular Diseases. 2018, 27(9): 2519-2523
26. Peng Yang, Anatol Manaenko, Feng Xu, et al. Role of PDGF-D and PDGFR-β in neuroinflammation in experimental ICH mice model. Experimental Neurology. 2016, 283 :157-164.
27. Yijun Cheng, Bin Chen, Wanqun Xie, et al. Ghrelin attenuates secondary brain injury following intracerebral hemorrhage by inhibiting NLRP3 inflammasome activation and promoting Nrf2/ARE signaling pathway in mice. International Immunopharmacology. 2020, 79: 106180
28. Che-Feng Chang, Jieru Wan, Qiang Li, et al. Alternative activation-skewed microglia/macrophages promote hematoma resolution in experimental intracerebral hemorrhage. Neurobiology of Disease. 2017, 103: 54-69.
29. Gui-yun Cui, Xiu-ming Gao, Su-hua Qi, et al. The action of thrombin in intracerebral hemorrhage induced brain damage is mediated via PKCα/PKCδ signaling. Brain Research. 2011, 1398(29): 86-93
30. Yu Zhou, Yanchun Wang, Jian Wang, et al. Inflammation in intracerebral hemorrhage: From mechanisms to clinical translation. Progress in Neurobiology. 2014. 115: 25-44.
31. X. Xu, J. Zhang, X. Chen, et al. The increased expression of metabotropic glutamate receptor 5 in subventricular zone neural progenitor cells and enhanced neurogenesis in a rat model of intracerebral hemorrhage Neuroscience. 2012, 202(27): 474-483.
32. Yang Zhang, Tianfeng Huang, Lulu Jiang, et al. MCP-induced protein 1 attenuates sepsis-induced acute lung injury by modulating macrophage polarization via the JNK/c-Myc pathway. International Immunopharmacology. 2019. 75; 105741.
33. Rukmani Sridharan, Brenton Cavanagh, Andrew R. Cameron, et al. Material stiffness influences the polarization state, function and migration mode of macrophages. Acta Biomaterialia. 2019. 8915: 47-59
34. Evan Trus, Sameh Basta, Katrina Gee. Who's in charge here? Macrophage colony stimulating factor and granulocyte macrophage colony stimulating factor: Competing factors in macrophage polarization. Cytokine. 2020. 127: 154939

35. Debora Scaldaferri, Annalisa Bosi, Marco Fabbri, et al. The human RNASET2 protein affects the polarization pattern of human macrophages in vitro. Immunology Letters. 2018.203: 102-111.
36. Chunyan Wang, Michael C. Petriello, Beibei Zhu, et al. PCB 126 induces monocyte/macrophage polarization and inflammation through AhR and NF-κB pathways. Toxicology and Applied Pharmacology. 2019, 367(15): 71-81.
37. Min Qiu, Junbing Ma, Juan Zhang, et al. MicroRNA-150 deficiency accelerates intimal hyperplasia by acting as a novel regulator of macrophage polarization. Life Sciences. 240(1): 116985.
38. Juan Hu, Cong-Xin Huang, Pan-Pan Rao, et al. Inhibition of microRNA-155 attenuates sympathetic neural remodeling following myocardial infarction via reducing M1 macrophagepolarization and inflammatory responses in mice. European Journal of Pharmacology. 2019. 851(15): 122-132.
39. Dan Li, Mingyue Duan, Yuan Feng, et al. MiR-146a modulates macrophage polarization in systemic juvenile idiopathic arthritis by targeting INHBA. Molecular Immunology. 2016. 77: 205-212.
40. Yuanyuan An, Qing Yang. MiR-21 modulates the polarization of macrophages and increases the effects of M2 macrophages on promoting the chemoresistance of ovarian cancer. Life Sciences. 2020, 242(1) :117162.
41. Hua-bin Zhang, Xian-kun Tu, Quan Chen, et al. Propofol Reduces Inflammatory Brain Injury after Subarachnoid Hemorrhage: Involvement of PI3K/Akt Pathway Journal of Stroke and Cerebrovascular Diseases. 2019. 28(12): 104375.
42. Hong-jie Xi, Tian-hua Zhang, Tao Tao, et al. Propofol improved neurobehavioral outcome of cerebral ischemia–reperfusion rats by regulating Bcl-2 and Bax expression. Brain Research. 2011. 1410(2): 24-32.

Figures

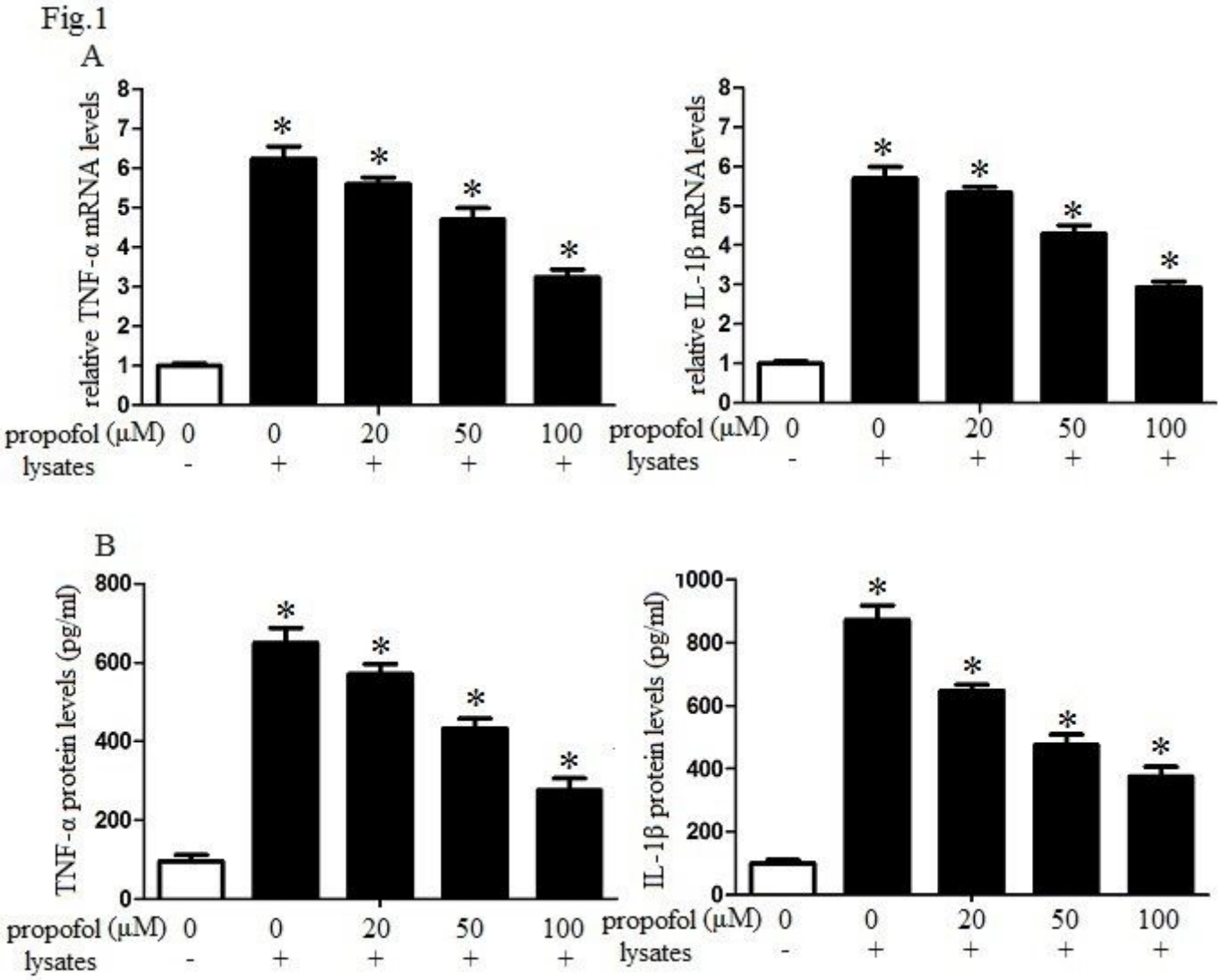

Figure 1

Propofol attenuates erythrocyte lysates-induced M1 polarization. Macrophages (1×105) were stimulated with propofol (0-100 μM) plus 10μl erythrocyte lysates for 24 hs. (A) The cells were collected and homogenized, TNF-α and IL-1β mRNA were analyzed by qRT-PCR assay. (B) The cell supernatants were harvested, and TNF-α and IL-1β productions were determined by ELISA. Experiments performed in triplicate showed consistent results. Data are presented as the mean ± standard error of mean (SEM) of three independent experiments. *P < 0.05

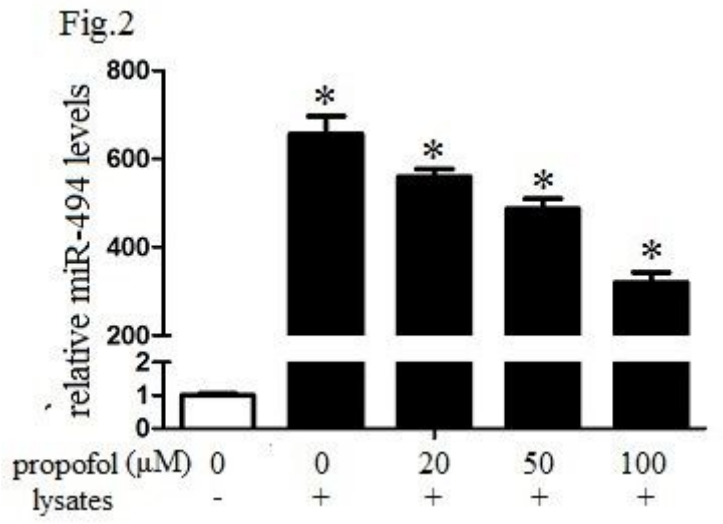

Figure 2

Propofol suppresses erythrocyte lysates-induced miR-494 levels. Macrophages (1×105) were stimulated with propofol (0-100 μM) plus 10μl erythrocyte lysates for 24 hs. The cells were collected and homogenized, miR-494 levels were analyzed by qRT-PCR assay. Experiments performed in triplicate showed consistent results. Data are presented as the mean ± standard error of mean (SEM) of three independent experiments. *P < 0.05

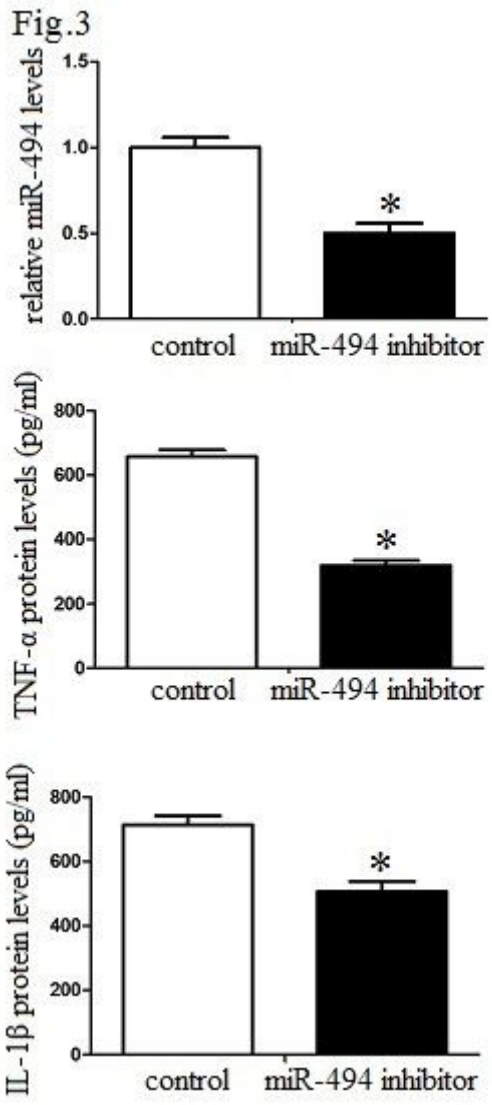

Figure 3

MiR-494 is required for propofol inhibition of inflammation. (A) Macrophages (1×105) were transduced with miR-494 inhibitor (50 nmol/L) or control for 24 hs. The cells were collected and homogenized, miR-494 levels were analyzed by qRT-PCR assay. (B) Macrophages (1×105) were transduced with miR-494 inhibitor (50 nmol/L) or control for 24 hs, then cells were stimulated with propofol (100 μM) plus 10μl erythrocyte lysates for 24 hs. The cell supernatants were harvested, and TNF-α and IL-1β productions were determined by ELISA. Experiments performed in triplicate showed consistent results. Data are presented as the mean ± standard error of mean (SEM) of three independent experiments. *P < 0.05

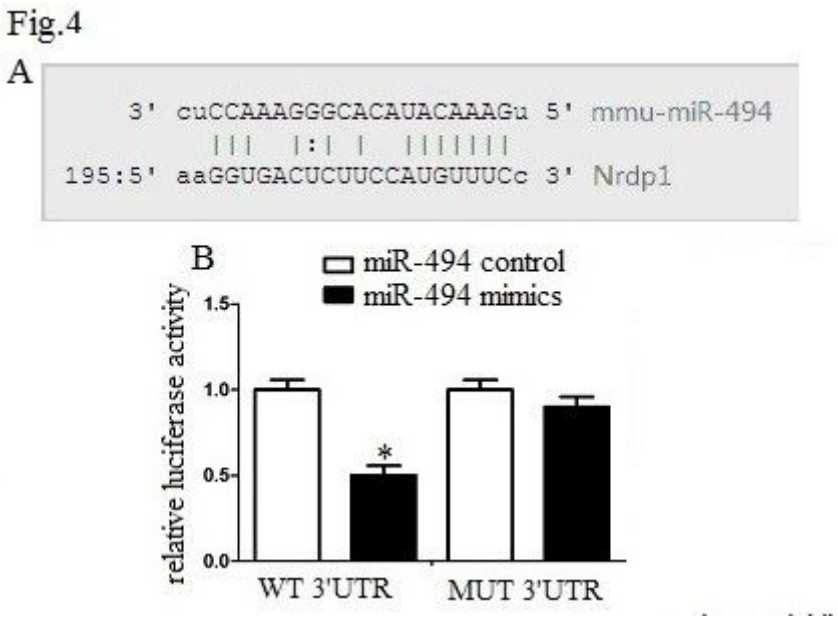

Figure 4

Nrdp1 was a direct target of miR-494 in macrophage (A) The region of the Nrdp1 mRNA 3'UTR predicted to be targeted by miR-494 as indicated. (B) Luciferase activity assays using reporters with wild-type or mutant Nrdp1 3'UTRs were performed after cotransfection with miR-494 mimics or control in macrophage.

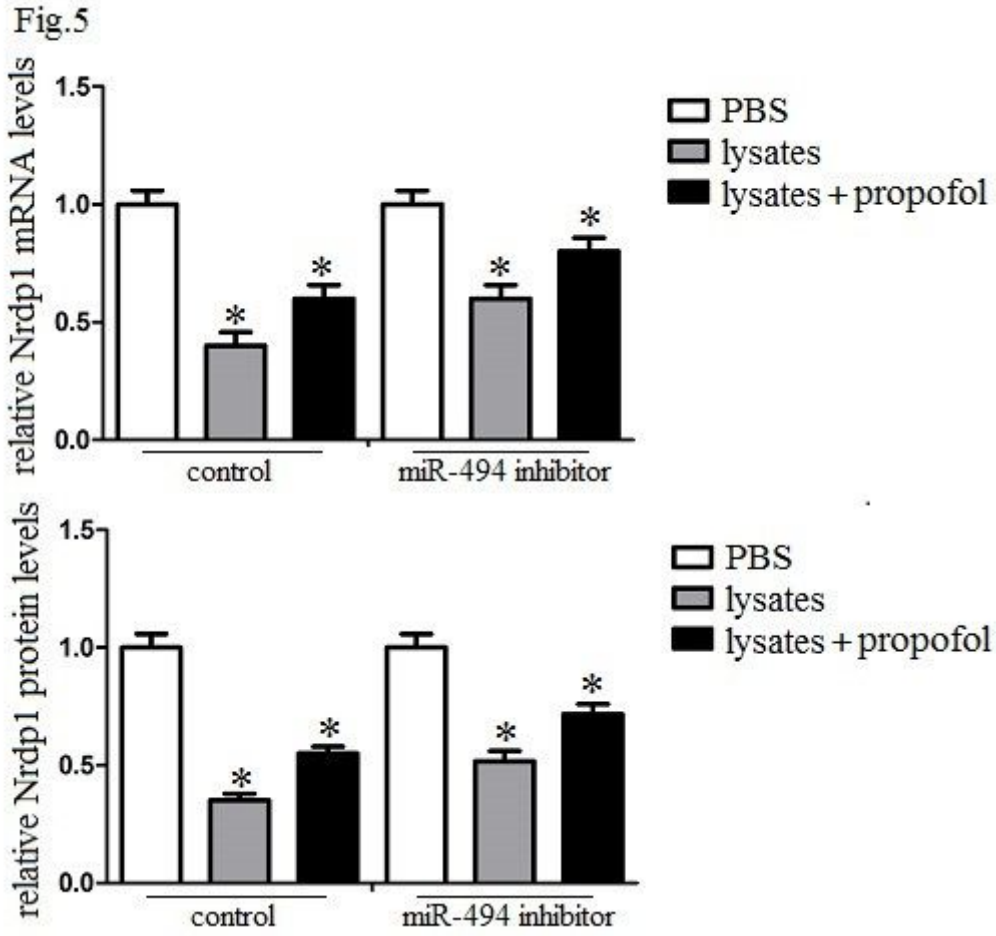

Figure 5

Propofol upregulates Nrdp1 by suppressing miR-494 Macrophages (1×105) were transduced with miR-494 inhibitor (50 nmol/L) or control for 24 hs, then cells were stimulated with PBS, erythrocyte lysates or erythrocyte lysates plus propofol (100 μM) for 24 hs. The cells were collected and homogenized, Nrdp1 levels were analyzed by qRT-PCR and western blot assays. Experiments performed in triplicate showed consistent results. Data are presented as the mean ± standard error of mean (SEM) of three independent experiments. *P < 0.05

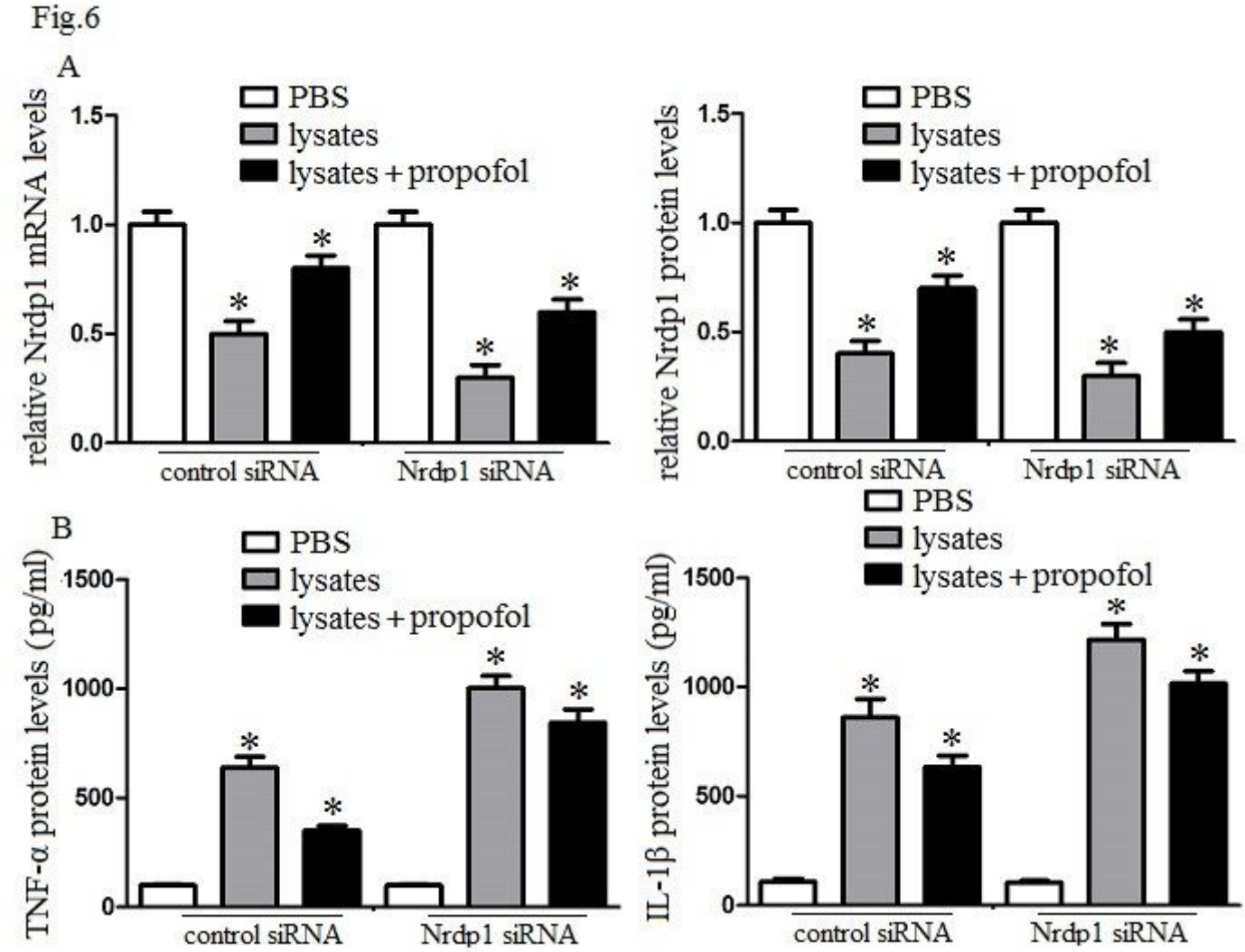

Figure 6

Downregulation of Nrdp1 attenuates the anti-inflammatory effects of propofol. (A) Macrophages (1×105) were transduced with Nrdp1 siRNA or control siRNA, then cells were stimulated with PBS, erythrocyte lysates or erythrocyte lysates plus propofol (100 μM) for 24 hs. The cells were collected and homogenized, Nrdp1 levels were analyzed by qRT-PCR and western blot assays. (B) Macrophages (1×105) were transduced with Nrdp1 siRNA or control siRNA, then cells were stimulated with PBS, erythrocyte lysates or erythrocyte lysates plus propofol (100 μM) for 24 hs. The cell supernatants were harvested, and TNF-α and IL-1β productions were determined by ELISA. Experiments performed in

triplicate showed consistent results. Data are presented as the mean ± standard error of mean (SEM) of three independent experiments. *P < 0.05

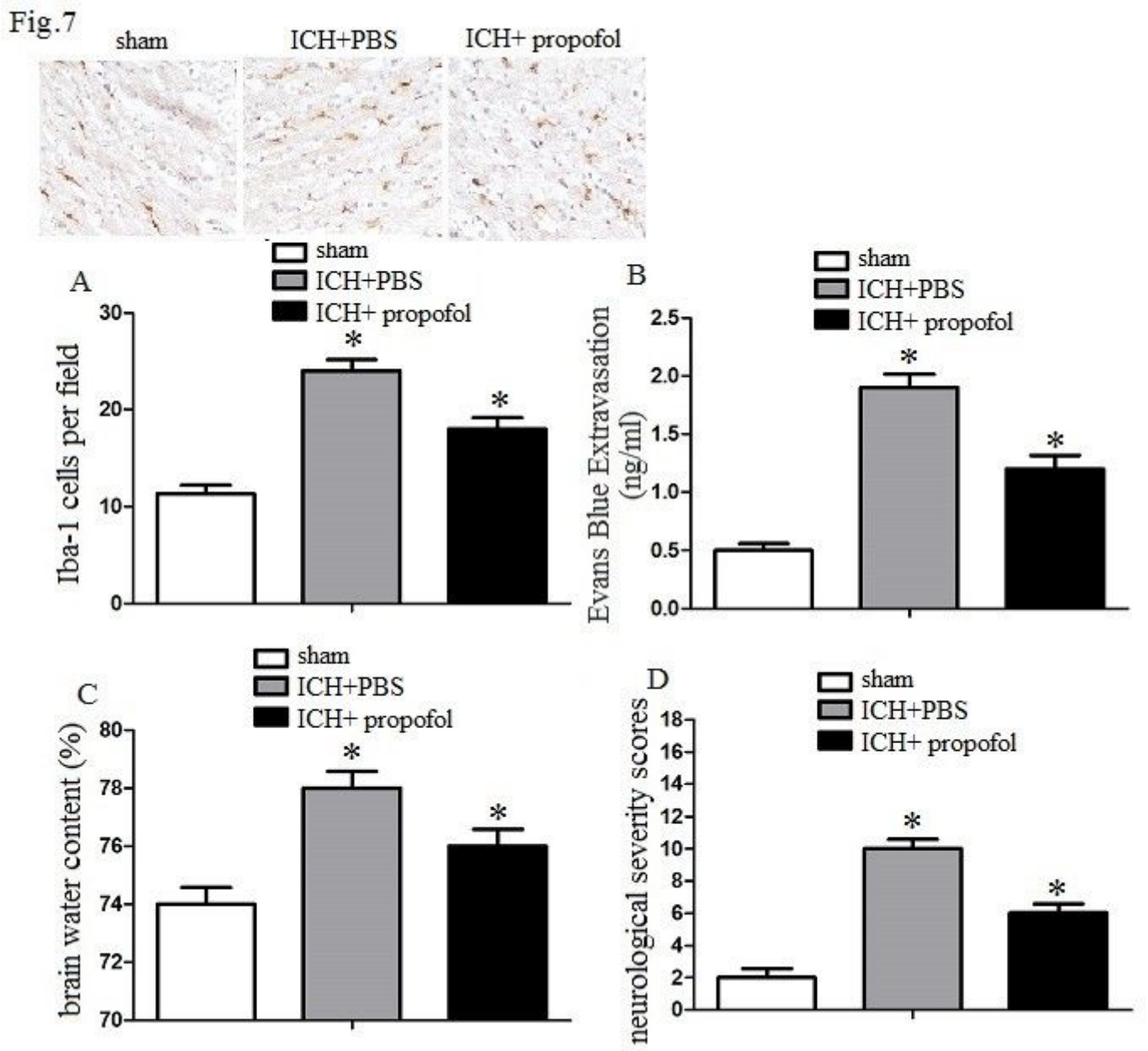

Figure 7

Propofol inhibits inflammatory injury in vivo. After 3 days post ICH, mice (n = 10 per group) were deeply anesthetized in a transcardial manner. (A) The brains were removed and post fixed. The perihematomal region of cerebral tissue was collected, and macrophages were analyzed with anti-Iba-1 antibody (×400 magnification). (B) The BBB disruption of mice (n=10 per group) was analyzed. (C) The cerebral water content of mice (n=10 per group) was also analyzed. (D) The neurological deficit tests were performed by behavioral measurement, including composite of motor, sensory, reflex, and balance tests. Experiments performed in triplicate showed consistent results. Data are presented as the mean ± standard error of mean (SEM) of three independent experiments. *P < 0.05